Z. Angew. Math. Phys. (2016) 67:122
© 2016 Springer International Publishing
0044-2275/16/050001-16
published online September 17, 2016
DOI 10.1007/s00033-016-0713-4

Zeitschrift für angewandte Mathematik und Physik ZAMP

Non-standard coupled extensional and bending bias tests for planar pantographic lattices. Part I: numerical simulations

Emilio Turco, Katarzyna Barcz, Marek Pawlikowski and Nicola Luigi Rizzi

Abstract. In dell'Isola et al. (Zeitschrift für Angewandte Math und Physik 66(6):3473–3498, 2015, Proc R Soc Lond A Math Phys Eng Sci 472(2185):1–23, 2016), the concept of pantographic sheet is proposed. The aim is to design a metamaterial showing: (i) a large range of elastic response; (ii) an extreme toughness in extensional deformation; (iii) a convenient ratio between toughness and weight. However, these required properties must coexist with non-detrimental mechanical characteristics in the presence of other kinds of imposed displacements. The aim of this paper is to prove *via* numerical simulations that pantographic sheets may effectively resist to coupled bending and extensional deformations. The four-parameter model introduced shows its versatility as it is able to encompass all the considered types of (large) deformations. The numerical integration scheme which we use is based on the same concepts exploited in Turco et al. (Zeitschrift für Angewandte Math und Physik 67(4):1–28, 2016): They prove that the Hencky-type discretization is very efficient also in nonlinear large deformations and large displacements regimes. In Part II of this paper, we will show that the used models are very effective to describe experimental evidence.

Mathematics Subject Classification. Primary 74-XX; Secondary 70H03, 74-04, 74B20, 74S30, 74Q05.

Keywords. Pantographic structures, Micro-mechanical model, Second gradient continuum, Nonlinear problems.

1. Introduction

In [1] and [2], the concept of pantographic sheet is proposed. This fabric was exploited in more theoretical papers [4–6] to prove that there exists a fabric whose macro-continuum model is not a first gradient one. However, it revealed itself to have very interesting properties, so that from a different point of view it can be regarded as a metamaterial enjoying very peculiar properties, including at least:

1. a surprisingly large range of elastic response;
2. an extreme toughness in extensional deformation;
3. a convenient ratio between toughness and weight.

On the other hand, these very positive properties should not coexist with very detrimental other mechanical or physical characteristics in the presence of other kinds of imposed displacements or of any kind of frequent external actions. Therefore, a systematic series of investigations is needed to establish whether there are some contraindications to the use of pantographic fabrics in composites or in other engineering applications.

The aim of this paper is to start this kind of investigations and in particular to start to assess, both via numerical simulations and by means of experimental measurements, that pantographic sheets can effectively resist to imposed displacements producing coupled bending and extensional deformations.

It has to be remarked that: (i) the introduced models are strongly nonlinear, so that they show strong coupling between different deformation modes; in particular, extensional deformation may (and do) affect bending deformation of pantographic sheets; (ii) the physical experimental evidence shows (see part II) that such strong coupling phenomena are really relevant; (iii) the four-parameter models introduced show a very promising versatility; indeed they are able, without changing the values of the material

parameters previously attributed in simple extensional tests to a specific specimen, to encompass also more general types of deformation. The numerical results were so promising that a campaign of experimental measurements was started: In Part II, it will be seen that all available experimental evidence does not show any detrimental feature of pantographic sheets in the types of deformation which we consider theoretically here.

In next sections will be considered: (i) some relevant theoretical and modeling assumptions, (ii) an effective numerical procedure allowing for the determination of the equilibrium shapes of pantographic sheets based on Hencky-type discretization, (iii) a numerical procedure based on FEM discretizing a second gradient continuum model for pantographic sheets and (iv) the careful comparison of the performances and results obtained in points (iii) and (ii).

In particular, in Sect. 2 will be briefly sketched the main points of the macro-description (continuum to be discretized via FEM) and meso-description (directly a discrete model); in Sect. 3 will be presented and thoroughly discussed the results of the continuum and the discrete model which will allow for an accurate comparison with the experimental tests; finally, in Sect. 4, there are some concluding remarks and future perspectives.

2. Deformation energies in meso-(discrete) and in macro-(continuum) descriptions

In this Section, we shortly specify the discrete and the continuum models which seem to be the most suitable to design the experimental setup. They will be applied in the Part II, in order to explain the results of experimental evidence.

It has to be remarked here that: (i) it became rather easy, by using 3D printing technologies (see Fig. 1) to built pantographic lattices; they were conceived (on the basis concept first proposed in [1] as constituted by two arrays of beams (colored in green and blue in Fig. 1) interconnected by elastic pivots realized with small-size elastic cylinders (in red in Fig. 1); (ii) discrete model and continuum models can be introduced for modeling their behavior, and their respective applicability ranges, while not completely overlapping, have a large intersection; we will explore in this paper how large is this intersection.

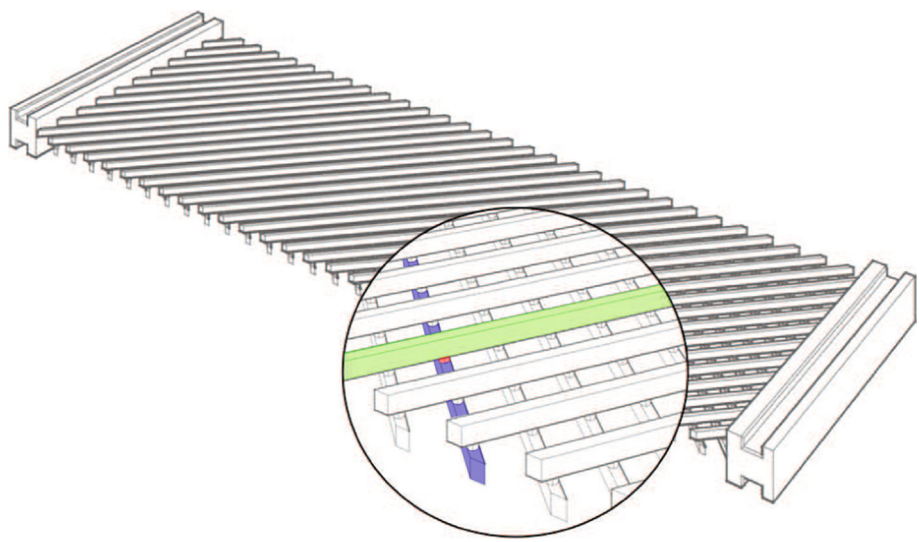

FIG. 1. Pantographic structure built by using 3D printing technology: two non-parallel fibers are *colored* in *blue* and *green*, the corresponding pivot is in *red* (color figure online)

2.1. Discrete and continuous kinematics

The kinematical descriptions introduced differ depending on the used model. Indeed:

- the discrete model specifies the position of all the material particles modeling the pivots; these particles are identified with the nodes of the reference configuration and need to be displaced to the actual configuration. If N is the number of involved particles, each of which is denoted by $P_{i,j}$, then the set of Lagrangian coordinates can be given by their actual positions $p_{i,j}$;
- the continuous model specifies a regular field χ (at least C^0 its further regularity being dictated by the postulated deformation energy) defined in the reference configuration and mapping a generic material particle in its actual position.

Piola's Ansatz, see [7], consists in assuming that the correspondence between discrete and continuous model is given, see also [2], by:

$$\chi(P_{i,j}) = p_{i,j}. \tag{1}$$

2.2. Discrete and continuous energies

Total deformation energy, in hard devices induced deformations (and in the absence of relevant volume forces), reduces to the deformation energies only. Therefore, in both discrete and continuous models they are the only kind of energy to be specified.

The postulated expression for the Lagrangian discrete deformation energy, see [3,8] for a comprehensive description (in terms of the Lagrangian coordinates $p_{i,j}$), is given by:

$$\begin{aligned} E\left(\{p_{i,j}\}\right) = {} & \frac{1}{2}\sum_i\sum_j a_{i,j}^{(\alpha_1)}\left(\|p_{i+1,j}-p_{i,j}\|-\varepsilon\right)^2 + \sum_i\sum_j a_{i,j}^{(\alpha_2)}\left(\|p_{i,j+1}-p_{i,j}\|-\varepsilon\right)^2 \\ & + \sum_i\sum_j b_{i,j}^{(\alpha_1)}\left(\cos\vartheta_{i,j}^{(\alpha_1)}+1\right) + \sum_i\sum_j b_{i,j}^{(\alpha_2)}\left(\cos\vartheta_{i,j}^{(2)}+1\right) \\ & + \frac{1}{2}\sum_i\sum_j s_{i,j}\left(\vartheta_{i,j}^{(s)}-\frac{\pi}{2}\right)^2, \end{aligned} \tag{2}$$

where the first two addends are related to the extensional energy of the fibers in α_m-directions ($m=1,2$), see Figs. 2 and 3, being $a_{i,j}^{(\alpha_m)}$ the extensional stiffness parameters in α_m-direction; the second two ones to the bending energy of the fibers, again in α_m-direction, having used the bending stiffness parameter $b_{i,j}^{(\alpha_m)}$; the last contribution is instead related to the shear energy of the springs with stiffness parameter $s_{i,j}$.

Instead, the expression for the second gradient Piola's deformation energy in the continuum model (in terms of the placement field χ), see [2] for a depth insight, is given by:

$$\begin{aligned} E\left(\chi\right) = {} & \frac{1}{2}\int_\Omega \sum_{\alpha_m} A^{(\alpha_m)}\left(\|\mathbf{F}\mathbf{d}_{\alpha_m}\|-1\right)^2 \mathrm{d}\Omega \\ & + \frac{1}{2}\int_\Omega \sum_{\alpha_m} B^{(\alpha_m)}\left(\frac{\nabla\mathbf{F}|\mathbf{d}_{\alpha_m}\otimes\mathbf{d}_{\alpha_m}\cdot\nabla\mathbf{F}|\mathbf{d}_{\alpha_m}\otimes\mathbf{d}_{\alpha_m}}{\|\mathbf{F}\mathbf{d}_{\alpha_m}\|^2} - \left(\frac{\mathbf{F}\mathbf{d}_{\alpha_m}}{\|\mathbf{F}\mathbf{d}_{\alpha_m}\|}\cdot\frac{\nabla\mathbf{F}|\mathbf{d}_{\alpha_m}\otimes\mathbf{d}_{\alpha_m}}{\|\mathbf{F}\mathbf{d}_{\alpha_m}\|}\right)^2\right)\mathrm{d}\Omega \\ & + \frac{1}{2}\int_\Omega S\left(\arccos\left(\frac{\mathbf{F}\mathbf{d}_{\alpha_1}}{\|\mathbf{F}\mathbf{d}_{\alpha_1\|}}\cdot\frac{\mathbf{F}\mathbf{d}_{\alpha_2}}{\|\mathbf{F}\mathbf{d}_{\alpha_2}\|}\right)-\frac{\pi}{2}\right)^2\mathrm{d}\Omega\,, \end{aligned} \tag{3}$$

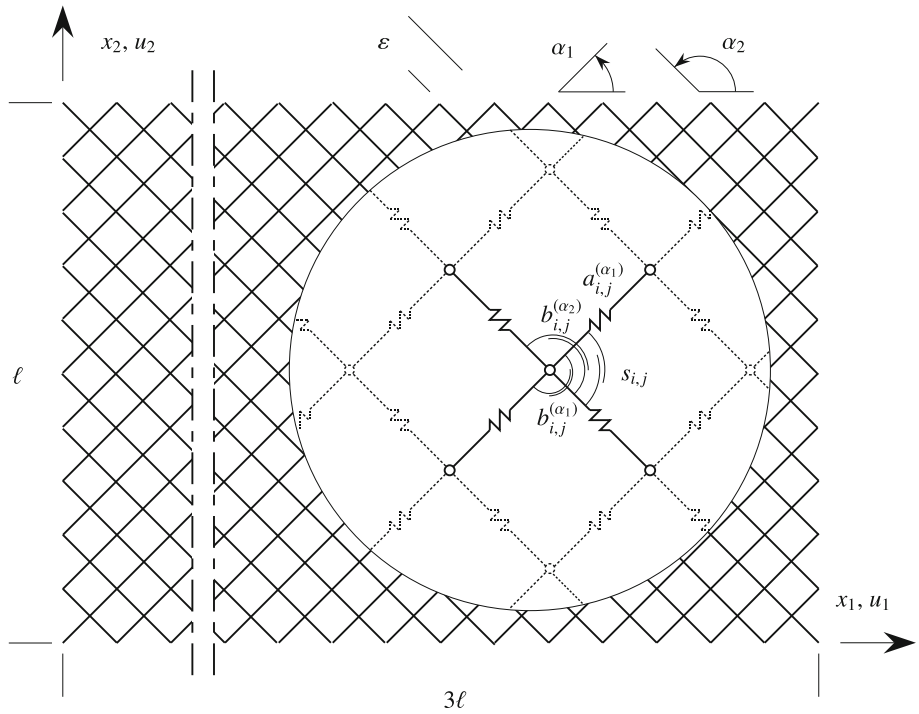

FIG. 2. Hencky-type mechanical model of pantographic structure

where the stiffness parameters of the continuum model (macro) $A^{(\alpha_m)}, B^{(\alpha_m)}$ and S are related to the stiffness parameters of the discrete model (meso) $a_{i,j}^{(\alpha_m)}, b_{i,j}^{(\alpha_m)}$ and $s_{i,j}$ as follows:

$$\begin{aligned} A^{(\alpha_m)} &= a_{i,j}^{(\alpha_m)}\,, \\ B^{(\alpha_m)} &= b_{i,j}^{(\alpha_m)}\,, \\ S &= \frac{s_{i,j}}{\varepsilon^2}\,, \end{aligned} \tag{4}$$

and having used the notation

$$\mathbf{F} = \nabla\chi\,, \tag{5}$$

$$(\nabla\mathbf{F}|\mathbf{d}_{\alpha_m} \otimes \mathbf{d}_{\alpha_m})^{\beta} = F^{\beta}_{\alpha_m,\alpha_m}\,, \quad \text{(no sum over repeated } \alpha_m \text{ is intended)} \tag{6}$$

Some remarks:

1. In [2], Eqs. (2) and (3) were written in a more general form by using for the shear strain term the exponent γ instead of 2; this is particularly useful to improve the fit of the experimental tests by theoretical models.
2. The shear springs used for the discrete model, and depicted in Figs. 2 and 3, are actually four, having the same stiffness, for each node or pivot, indicated $P_{i,j}$ in the reference configuration, one for each quadrant having origin in $P_{i,j}$.
3. The bending stiffness is expressed by means of the $\cos\vartheta_{i,j}^{(\alpha_m)}$ instead of the corresponding angle $\vartheta_{i,j}^{(\alpha_m)}$, and these two possibilities are equivalent, in principle, but the first, avoiding the uses of $\arccos(\cdot)$ function, results more convenient from the computational point of view since it produces a more compact and effective code.

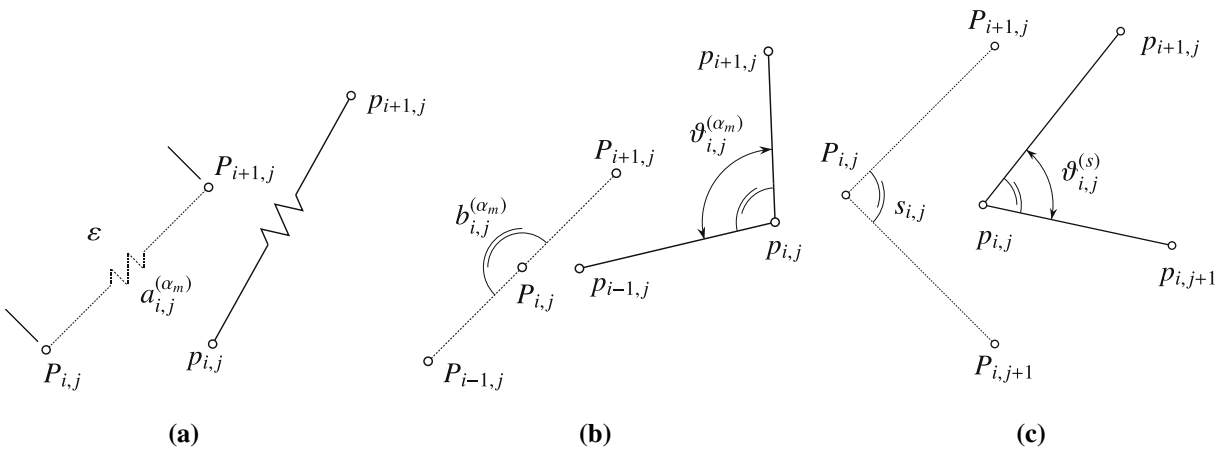

FIG. 3. Kinematics of extensional (a), bending (b) and shear (c) springs: reference and actual configurations

TABLE 1. *Stiffness parameters for extensional, $a_{i,j}^{(\alpha_m)}$, bending, $b_{i,j}^{(\alpha_m)}$, and shear, $s_{i,j}$, springs*

$a_{i,j}^{(\alpha_m)}$	$b_{i,j}^{(\alpha_m)}$	$s_{i,j}$
265.0 N/mm	238.2 Nmm	0.9739 Nmm

3. Numerical results deriving from discrete and continuum models

In order to check the numerical results deriving from the discrete and continuous model, we design some tests to perform with the two models and successively with experiments on specifically designed fabrics made by using the 3D printing technology in polyamide, see the companion paper [9].

By referring to Fig. 2, we assume for the geometrical parameters: $\ell = 69.3$ mm, $\varepsilon = 6.13$ mm, $\alpha_1 = \pi/4$ and $\alpha_2 = 3\pi/4$. Furthermore, we consider the case whose cross section of each fiber is a rectangle having a width equal to 2.25 mm and a depth equal to 1.6 mm and each pivot is a cylinder having a diameter equal to 0.9 mm and a height equal to 1 mm. For the polyamide, many experimental tests indicate that an appropriate value for the Young's modulus is 1600 MPa.

From the geometrical and mechanical parameters just described, the extensional, bending and shear spring stiffnesses were estimated by using the guidelines described in [10]. Consequently, for the numerical simulation reported in the sequel, we assume as stiffness parameters for each kind of used spring the values reported in Table 1.

It has to be underlined that this choice of the constitutive parameters, suggested by the numerical simulations concerning the extension bias test, see e.g. [3], is surely well calibrated for the continuum model but could be improved for the discrete model as it will be further discussed by referring to a particular numerical test at the end of this Section.

We consider here two set of imposed displacements which produce two kinds of coupled extensional and bending bias test: the first one determines a relative rigid rotation and translation of one side of the specimen with respect to the other (we will limit ourselves to the case in which the translation is parallel to the long side of the specimen in the reference configuration) and the second one imposes a displacement parallel to the long side of the specimen on a single fiber.

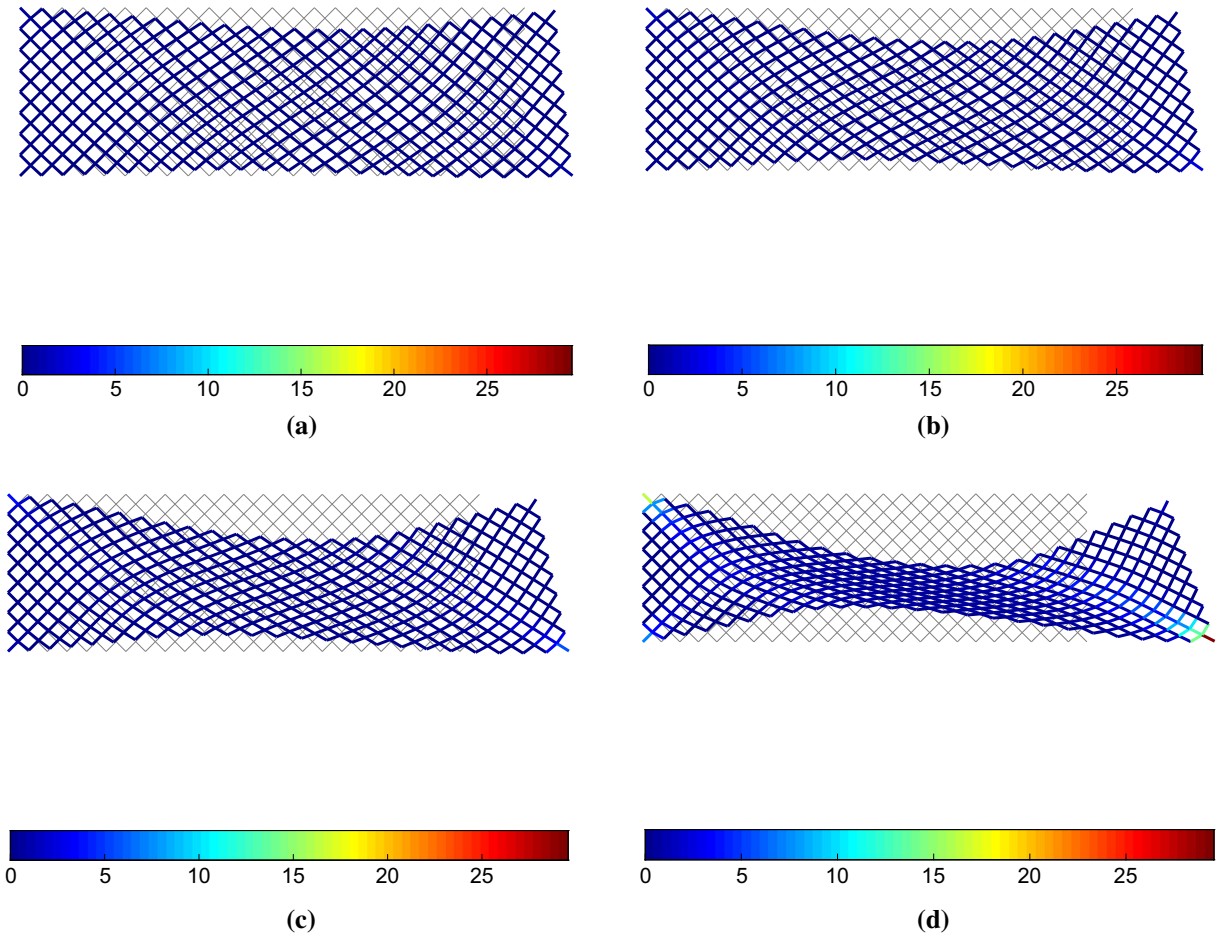

FIG. 4. Extensional and bending test simulation using the discrete model: deformation history varying the non-dimensional displacement parameter λ (in *grey* there is the reference solution, *colors* shows the energy level on the specimen) (color figure online)

3.1. Extensional and bending test

The first test, starting from the reference configuration, see Fig. 2, imposes, gradually, a coupled extensional and rotational displacement on the side having $x_1 = 3\ell$ until the maximum which, more specifically, is worth:

$$\begin{cases} u_1(3\ell, x_2) = u_1^{(0)} + (x_2 - e)\sin\beta\,, \\ u_2(3\ell, x_2) = -(x_2 - e)(1 - \cos\beta)\,, \end{cases} \tag{7}$$

where $u_1^{(0)} = 57.99$ mm, $e = \ell/12$ and $\beta = 18.48°$. The path between the initial (reference) and final configuration is governed by the non-dimensional displacement parameter λ which varies between $\lambda = 0$ for the reference configuration and $\lambda = 1$ for the final step.

The displacement described by Eq. 7 was used to compute, numerically, the structural response by using both the discrete and the continuum model described in the foregoing. Obviously, the results of continuum model derive from a suitable discretization by means of finite elements, see [2] for details.

The deformations obtained by the discrete model are reported in Fig. 4 using also in this case the non-dimensional displacement parameter λ where, besides the initial ($\lambda = 0$) and final configurations

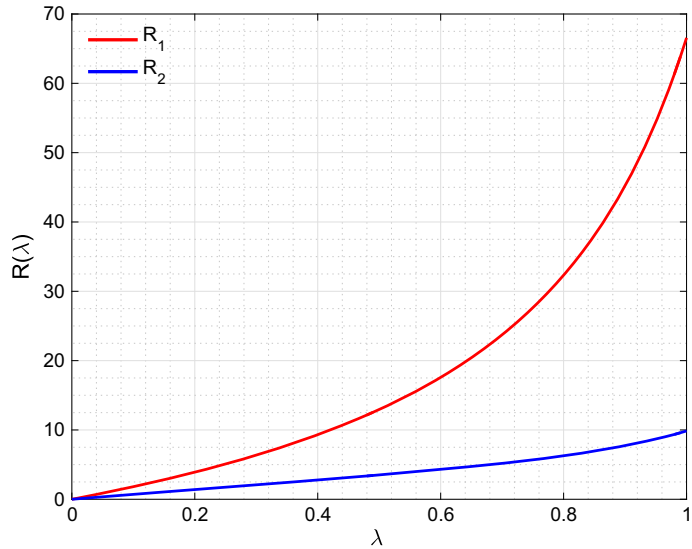

FIG. 5. Extensional and bending test simulation using the discrete model: global structural reaction R varying λ

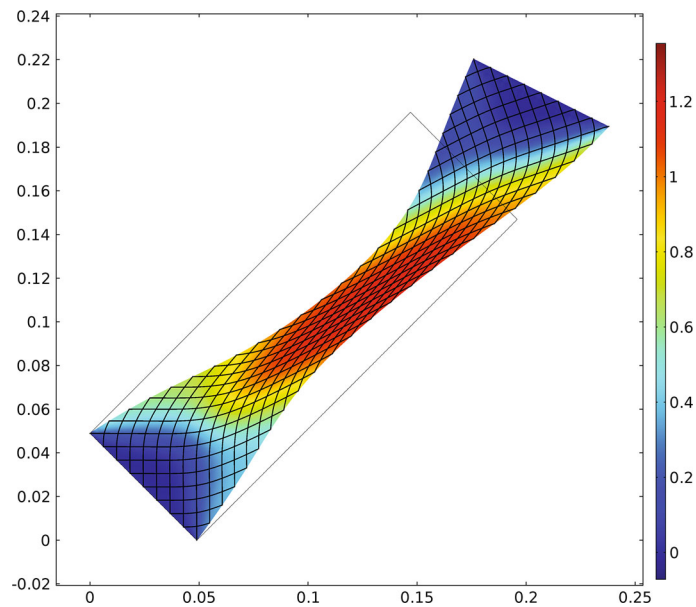

FIG. 6. Extensional and bending test simulation using the second gradient continuum model: deformation for $\lambda = 1$ (*colors* represent the angular strain between fibers)

($\lambda = 1$), there are reported three intermediate steps, precisely $\lambda = \frac{1}{3}, \frac{1}{2}, \frac{2}{3}$, the reference configuration is reported in gray in each one of the four images. The colors are used to give a clever representation of global energy level (extensional, bending and shear) on the pantographic structure.

Figure 5 reports the global structural reaction $R(\lambda)$ on the side $x_1 = 0$ evaluated by using the discrete model *via* numerical simulation, in red (R_1) and blue (R_2).

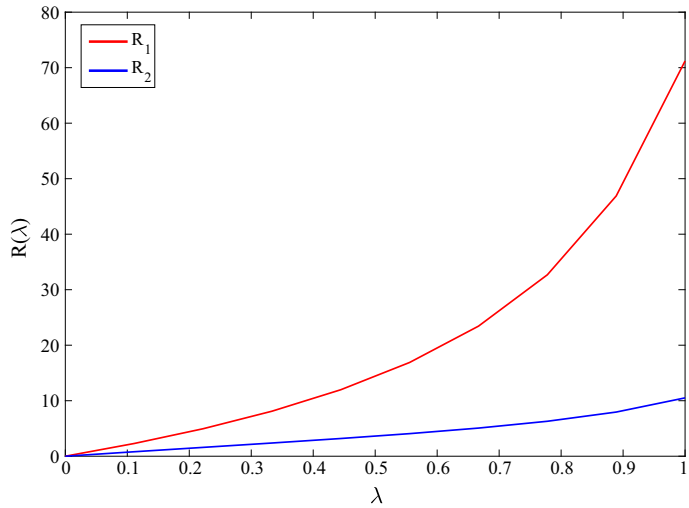

FIG. 7. Extensional and bending test simulation using the second gradient continuum model: global structural reaction R varying λ

For the same test, we report the results obtained by the second gradient continuum model, see Figs. 6 and 7. More precisely, in Fig. 6 there is the deformation corresponding to $\lambda = 1$ (colors, in this case, represent the angular strain between fibers) and in Fig. 7 the global structural reaction $R(\lambda)$ computed on the side $x_1 = 0$. We underline the good agreement between the results obtained by the two models for all the values of the non-dimensional displacement parameter λ.

3.2. Fiber extraction test

In this case, the coupling between extension and bending derives from a displacement imposed on a single fiber: starting from the reference configuration, a displacement v (on the upper right vertex), parallel to the longer side of the specimen, is gradually imposed on a single fiber until the value $v_{\max} = 78.0$ mm is achieved. The numerical simulation of this test, using the discrete model described in the foregoing, gives the plots reported in Fig. 8 using again the non-dimensional displacement parameter $\lambda = v/v_{\max}$ in order to distinguish both the intermediate and the final configurations, and using the colors to give evidence at a first glance to the energy level at each point of the pantographic structure.

As for the previous test, in Fig. 9 the global structural reaction $R(\lambda)$ on the side $x_1 = 0$, computed *via* numerical simulation, is reported, precisely the component R_1 in red and R_2 in blue.

For the same test, the results obtained by the second gradient continuum model, and after a suitable finite element discretization, are reported in Figs. 10 and 11. More precisely, in Fig. 10 there is the deformation at the final stage, $\lambda = 1$ (colors, also in this case, represent the angular strain between fibers), and in Fig. 11 the two components of the global structural reaction $R(\lambda)$. Also in this case, the results of the continuum model agree with those obtained from the discrete model (Figs. 8, 9).

3.3. Sensitivity analysis on the stiffness parameters for the discrete model

Finally, we report a basic sensitivity analysis with respect to the stiffness parameters $a_{i,j}^{(m)}, b_{i,j}^{(m)}$ and $s_{i,j}$ in order to remark the relevance of the correct identification of such parameters. Even though this first

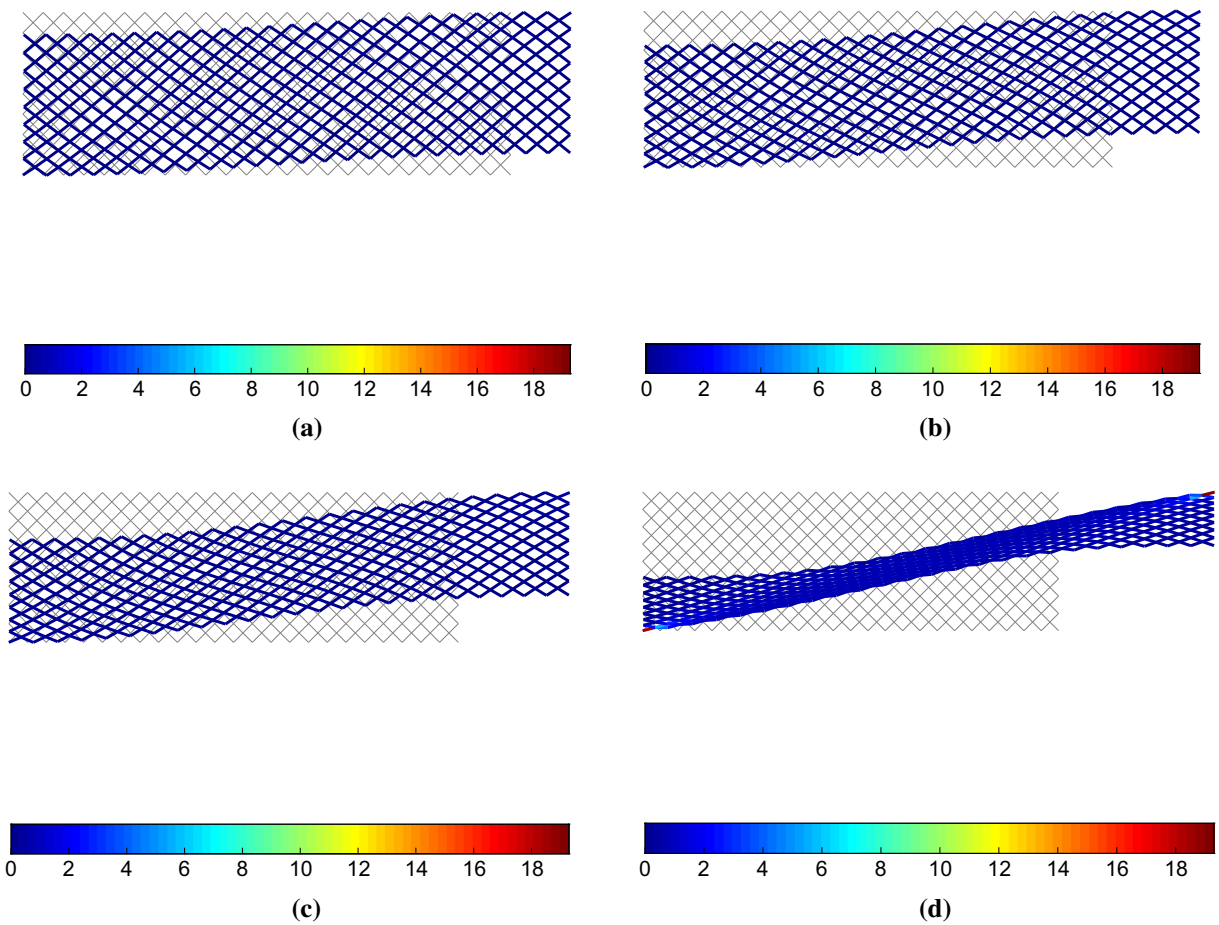

FIG. 8. Fiber extraction test simulation using the discrete model: deformation history varying λ (in *grey* there is the reference solution, *colors* shows the energy level) (color figure online)

tentative is surely insufficient to give reliable guidelines, it is capable to advise, also from a quantitative point of view, of the role played by the stiffness parameters.

To this aim, a series of analysis varying these parameters was performed choosing as output to check the history of the global structural reaction $R(\lambda)$ with respect to the non-dimensional displacement parameter λ. Here we report the results deriving from the extensional and bending test already presented and commented. More precisely, in Fig. 12 the global structural reaction $R(\lambda)$ is reported versus the non-dimensional parameter λ varying, one by one, the extensional $a_{i,j}^{(m)}$, the bending $b_{i,j}^{(m)}$ and the shear stiffness $s_{i,j}$ parameter. By assuming as reference values those reported in Table 1, the stiffness parameters were modified by means of the coefficients η_a, η_b and η_s each one halves or doubles the respective values of the stiffnesses.

Observing the curves reported in Fig. 12 and getting as reference the value reported in Table 1, when η_a, η_b and η_s move from 0.5 to 2, we remark that:

1. for the extensional parameter $a_{i,j}^{(m)}$, the variation ranges approximatively from -19 to 18 % for R_1 and -20 to 20 % for R_2;
2. for the bending parameter $b_{i,j}^{(m)}$, the variation ranges approximatively from -20 to 33 % for R_1 and -40 to 50 % for R_2;

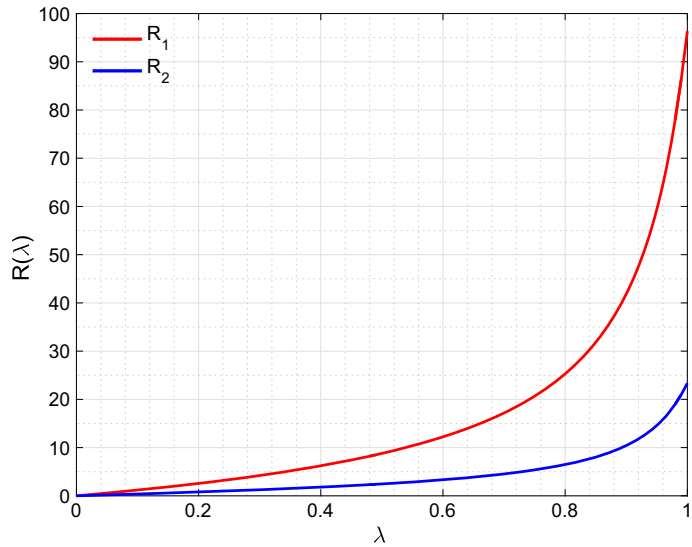

FIG. 9. Fiber extraction test simulation using the discrete model: global structural reaction R varying λ

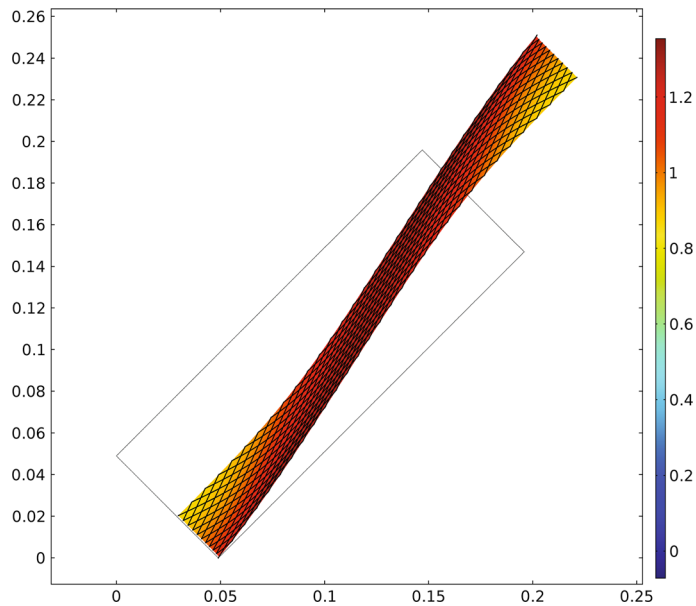

FIG. 10. Fiber extraction test: deformation for $\lambda = 1$ computed by the second gradient continuum model (*colors* represent the angular strain between fibers) (color figure online)

3. for the shear parameter $s_{i,j}$, the variation ranges approximatively from -18 to 36 % for R_1 and -20 to 20 % for R_2.

The basic analysis immediately above synthesized advises that the identification of the stiffness parameters requires great care in order to improve the results of the discrete model.

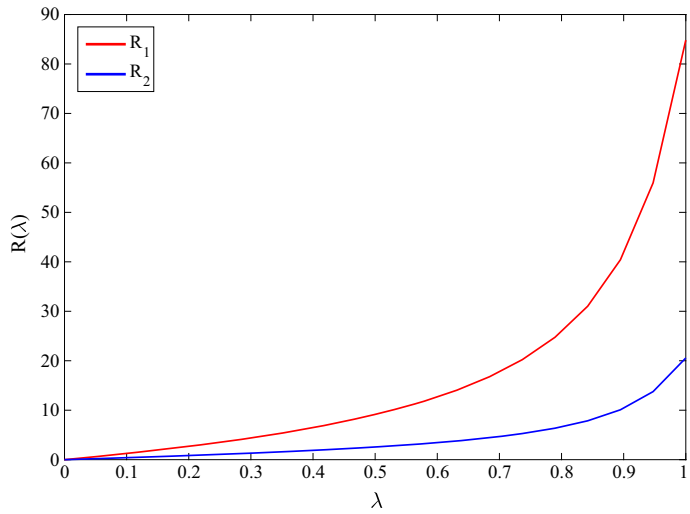

FIG. 11. Fiber extraction test: global structural reaction $R(\lambda)$ computed by using the second gradient continuum model

4. Conclusions and perspectives

The Part II of this paper will add to the theoretical results presented here the support of experimental evidence. We underline that the measurements presented in Part II were (as it has to be done) performed with the guidance and thanks to the understanding and insight obtained by means of the theoretical results: For these reasons, we presented them in the present Part I. The perspectives opened by presented results are of relevance. Indeed there is a strong motivation in continuing the investigations of the mechanical properties of pantographic sheets. Actually, it is needed to establish how they resist to:

(i) shear deformations (eventually coupled to extension and bending);
(ii) loads which are causing deformations out of plane and eventually buckling phenomena;
(iii) loads which are causing the onset of damage, damage evolution and eventually final failure.

Finally, it is needed to investigate the possibility to apply Castigliano's Theorem to pantographic sheets to obtain a global (and therefore robust) estimation of reactive forces in terms of total deformation energy.

As a consequence of the guidelines briefly exposed in the foregoing, we list some future perspectives of this research:

1. Pantographic structures were synthesized to give an example of second gradient metamaterial, see e.g. [11–22], modeled as generalized continua; this peculiarity generally produces accurate results using handy models; however in some specific deformation phenomena, the most appropriate models could not be those deriving from continuous theory. On the other hand, as seen in [2,7], when the qualitative description of their behavior is needed, then second gradient continuum models are surely more convenient.
2. Possible contact between fibers, observed in many experiments, could be addressed by using the guidelines reported in [23,24].
3. The construction of macro-springs obtained by using the capabilities of NURBS interpolation, see e.g. [25–32] in order to design new and enriched metamaterials. Also the capabilities of the generalized beam theory could furnish fruitful idea, see [33,34]. It is also very interesting the extension to the 3D case using the suggestions reported in [35].

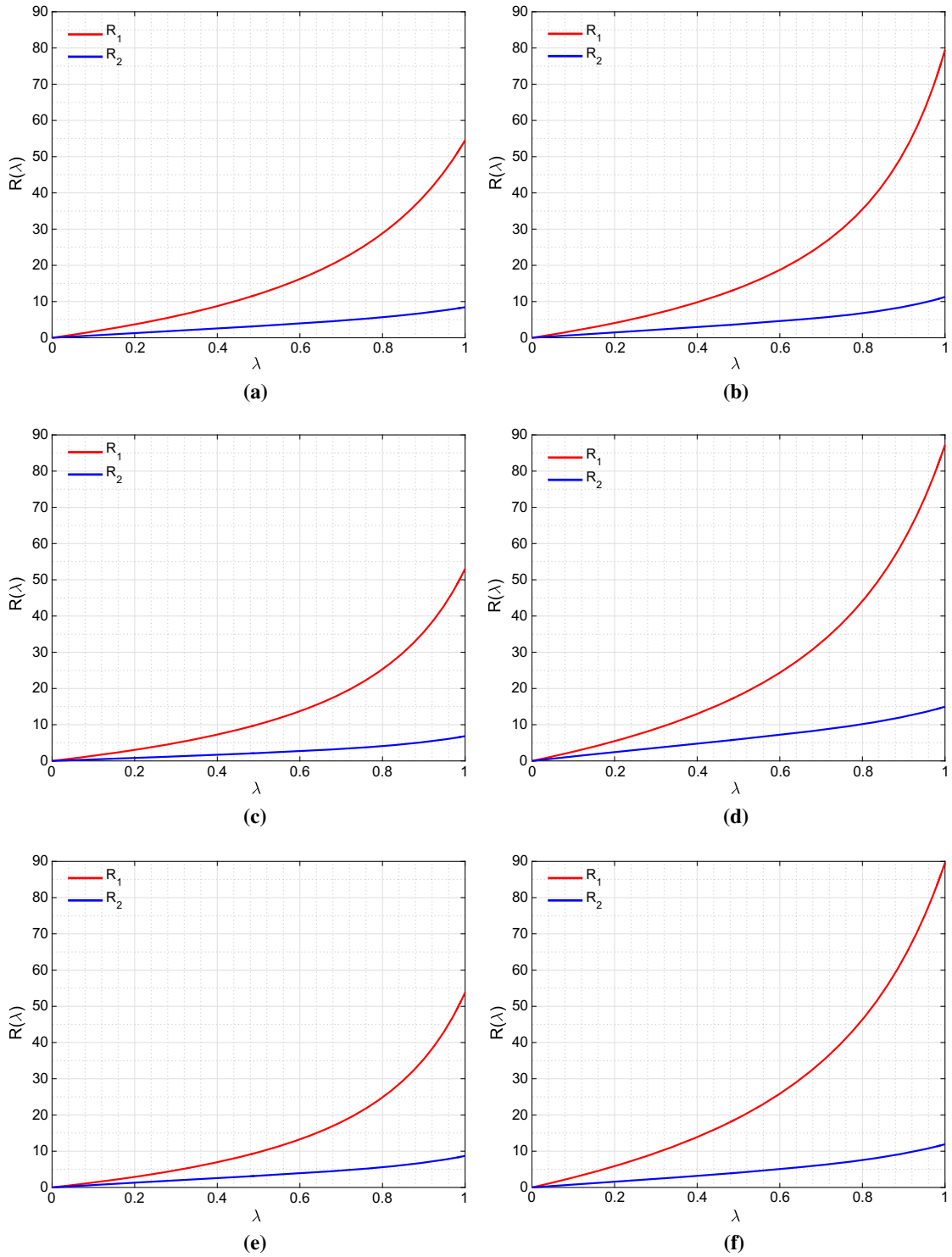

FIG. 12. Sensitivity analysis of global structural reaction $R(\lambda)$ versus the non-dimensional displacement parameter λ varying the stiffness parameters computed by using the discrete model

4. The Hencky-type model applied here to pantographic structure could also be used to model granular media interactions, see [36], or generalized continua, see [37–41] for a general review and [42–44] for applications in biomechanics and civil engineering. Furthermore, an analysis of the effects of imperfections, e.g. geometrical, on their mechanical behavior seems to be important, and this is related to the required further miniaturization of pantographic structures and the consequent unavoidable appearance of randomly distributed defects, see, e.g., the preliminary work [45].
5. The identification of the parameters of the discrete model, i.e. the stiffnesses of the springs, as briefly shown in Sect. 3 requires a specific investigation. In this direction, it could be useful to an extended sensitivity analysis on these parameters by using, for example, the tools reported in the review paper [46] and, in a detailed form, in [47–53], see also [54,55] for a specific application in problems concerning huge and innovative structures.
6. It appears interesting the extension to dynamic regimes, or, in other words, to consider the inertial forces, see some insight into the review paper [56] and also [57,58] for some general considerations.
7. The onset and the evolution of failure mechanisms involving, and observed in, pantographic sheets, as will be shown clearly in [9] for one of the cases studied here, involve ruptures concerning both fibers and pivots. A first tentative to solve this problem was presented in [59] obtaining results somewhat accurate when the failure mechanism concerning a fiber is activated. In this direction, it should also be considered the modeling of the out of plane deformation and the related buckling phenomena. The interested reader will find many interesting ideas in [60–70].

References

1. dell'Isola, F., Lekszycki, T., Pawlikowski, M., Grygoruk, R., Greco, L.: Designing a light fabric metamaterial being highly macroscopically tough under directional extension: first experimental evidence. Zeitschrift für Angewandte Math. Und Physik **66**(6), 3473–3498 (2015)
2. dell'Isola, F., Giorgio, I., Pawlikowski, M., Rizzi, N.L.: Large deformations of planar extensible beams and pantographic lattices: Heuristic homogenisation, experimental and numerical examples of equilibrium. Proc. R. Soc. Lond. A Math. Phys. Eng. Sci. **472**(2185), 1–23 (2016)
3. Turco, E., dell'Isola, F., Cazzani, A., Rizzi, N.L.: Hencky-type discrete model for pantographic structures: numerical comparison with second gradient continuum models. Zeitschrift für Angewandte Math. Und Physik **67**(4), 1–28 (2016)
4. Alibert, J.-J., Seppecher, P., dell'Isola, F.: Truss modular beams with deformation energy depending on higher displacement gradients. Math. Mech. Solids **8**(1), 51–73 (2003)
5. Seppecher, P., Alibert, J.-J., dell'Isola, F.: Linear elastic trusses leading to continua with exotic mechanical interactions. In: Journal of Physics: Conference Series, volume 319(1), p. 012018. IOP Publishing, (2011)
6. Alibert, J.-J., Della Corte, A.: Second-gradient continua as homogenized limit of pantographic microstructured plates: a rigorous proof. Zeitschrift für Angewandte Math. und Physik **66**, 2855–2870 (2015)
7. dell'Isola, F., Andreaus, U., Placidi, L.: At the origins and in the vanguard of peridynamics, non-local and higher-gradient continuum mechanics: An underestimated and still topical contribution of Gabrio Piola. Math. Mech. Solids **20**(8), 887–928 (2015)
8. Turco, E., Golaszewski, M., Cazzani, A., Rizzi, N.L.: Large deformations induced in planar pantographic sheets by loads applied on fibers: experimental validation of a discrete Lagrangian model. Mech. Res. Commun. **76**, 51–56 (2016)
9. Turco, E., Barcz, K., Rizzi, N.L.: Non-standard coupled extensional and bending bias tests for planar pantographic lattices. Part II: comparison with experimental evidence. Zeitschrift für Angewandte Math. und Physik, 1–16 (2016). doi:10.1007/s00033-016-0714-3
10. Placidi, L., Andreaus, U., Della Corte, A., Lekszycki, T.: Gedanken experiments for the determination of two-dimensional linear second gradient elasticity coefficients. Zeitschrift für Angewandte Math. Und Physik (ZAMP) **66**(6), 3699–3725 (2015)
11. dell'Isola, F., Steigmann, D., Della Corte, A.: Synthesis of fibrous complex structures: Designing microstructure to deliver targeted macroscale response. Appl. Mech. Rev. **67**(6), 060804 (2015)
12. Giorgio, I., Grygoruk, R., dell'Isola, F., Steigmann, D.J.: Pattern formation in the three-dimensional deformations of fibered sheets. Mech. Res. Commun. **69**, 164–171 (2015)
13. Scerrato, D., Giorgio, I., Rizzi, N.L.: Three-dimensional instabilities of pantographic sheets with parabolic lattices: numerical investigations. Zeitschrift für Angewandte Math. Und Physik **67**(3), 1–19 (2016)

14. Scerrato, D., Zhurba Eremeeva, I.A., Lekszycki, T., Rizzi, N.L.: On the effect of shear stiffness on the plane deformation of linear second gradient pantographic sheets. Zeitschrift für Angewandte Math. und Mechanik (2016). doi:10.1002/zamm.201600066
15. D'Agostino, M.V., Giorgio, I., Greco, L., Madeo, A., Boisse, P.: Continuum and discrete models for structures including (quasi-) inextensible elasticae with a view to the design and modeling of composite reinforcements. Int. J. Solids Struct. **59**, 1–17 (2015)
16. Placidi, L., Andreaus, U., Giorgio, I.: Identification of two-dimensional pantographic structure via a linear d4 orthotropic second gradient elastic model. J. Eng. Math. (2016). doi:10.1007/s10665-016-9856-8
17. Giorgio, I.: Numerical identification procedure between a micro Cauchy model and a macrosecond gradient model for planar pantographic structures. Zeitschrift für Angewandte Math. und Mechanik (2016). doi:10.1007/s00033-016-0692-5
18. Placidi, L., Dhaba, A.E.: Semi-inverse method à la Saint-Venant for two-dimensional linear isotropic homogeneous second-gradient elasticity. Math. Mech. Solids (2015). doi:10.1177/1081286515616043
19. dell'Isola, F., Giorgio, I., Andreaus, U.: Elastic pantographic 2d lattices: A numerical analysis on static response and wave propagation. Proc. Estonian Acad. Sci. **64**(3), 219–225 (2015)
20. dell'Isola, F., Della Corte, A., Greco, L., Luongo, A.: Plane bias extension test for a continuum with two inextensible families of fibers: A variational treatment with lagrange multipliers and a perturbation solution. Int. J. Solids Struct. **81**, 1–12 (2016)
21. Cuomo, M., dell'Isola, F., Greco, L.: Simplified analysis of a generalized bias test for fabrics with two families of inextensible fibres. Zeitschrift für Angewandte Math. Und Physik **67**(3), 1–23 (2016)
22. dell'Isola F., Cuomo M., Greco L., Della Corte A.: Bias extension test for pantographic sheets: numerical simulations based on second gradient shear energies. J. Eng. Math. (2016). doi:10.1007/s10665-016-9865-7
23. Andreaus, U., Baragatti, P., Placidi, L.: Soft-impact dynamics of deformable bodies. Contin. Mech. Thermodyn. **25**(3), 375–398 (2013)
24. Andreaus, U., Baragatti, P., Placidi, L.: Experimental and numerical investigations of the responses of a cantilever beam possibly contacting a deformable and dissipative obstacle under harmonic excitation. Int. J. Non-Linear Mech. **80**, 96–106 (2016)
25. Cazzani, A., Malagù, M., Turco, E.: Isogeometric analysis of plane curved beams. Math. Mech. Solids **21**(5), 562–577 (2016)
26. Cazzani, A., Malagù, M., Turco, E.: Isogeometric analysis: a powerful numerical tool for the elastic analysis of historical masonry arches. Contin. Mech. Thermodyn. **28**(1), 139–156 (2016)
27. Cazzani, A., Malagù, M., Turco, E., Stochino, F.: Constitutive models for strongly curved beams in the frame of isogeometric analysis. Math. Mech. Solids **21**(2), 182–209 (2016)
28. Bilotta, A., Formica, G., Turco, E.: Performance of a high–continuity finite element in three–dimensional elasticity. Int. J. Numer. Methods Biomed. Eng. **26**, 1155–1175 (2010)
29. Greco, L., Cuomo, M.: B-Spline interpolation of Kirchhoff–Love space rods. Comput. Methods Appl. Mech. Eng. **256**, 251–269 (2013)
30. Greco, L., Cuomo, M.: An implicit G^1 multi patch B-spline interpolation for Kirchhoff-Love space rod. Comput. Methods Appl. Mech. Eng. **269**, 173–197 (2014)
31. Greco, L., Cuomo, M.: An isogeometric implicit G1 mixed finite element for Kirchhoff space rods. Comput. Methods Appl. Mech. Eng. **298**, 325–349 (2016)
32. Cazzani, A., Stochino, F., Turco, E.: An analytical assessment of finite elements and isogeometric analysis of the whole spectrum of Timoshenko beams. Zeitschrift für Angewandte Math. und Mechanik (2016). doi:10.1002/zamm.201500280
33. Piccardo, G., Ranzi, G., Luongo, A.: A complete dynamic approach to the generalized beam theory cross-section analysis including extension and shear modes. Math. Mech. Solids **19**(8), 900–924 (2014)
34. Piccardo, G., Ranzi, G., Luongo, A.: A direct approach for the evaluation of the conventional modes within the gbt formulation. Thin-Walled Struct. **74**, 133–145 (2014)
35. Steigmann, D.J., Faulkner, M.G.: Variational theory for spatial rods. J. Elast. **33**(1), 1–26 (1993)
36. Misra, A., Poorsolhjouy, P.: Granular micromechanics based micromorphic model predicts frequency band gaps. Contin. Mech. Thermodyn. **28**(1), 215–234 (2016)
37. Altenbach, J., Altenbach, H., Eremeyev, V.A.: On generalized Cosserat-type theories of plates and shells: a short review and bibliography. Arch. Appl. Mech. **80**(1), 73–92 (2010)
38. Eremeyev, V.A., Pietraszkiewicz, W.: Material symmetry group and constitutive equations of micropolar anisotropic elastic solids. Math. Mechan. Solids (2015). (doi:10.1177/1081286515582862)
39. Dos Reis, F., Ganghoffer, J.F.: Construction of micropolar continua from the asymptotic homogenization of beam lattices. Comput. Struct. **112**, 354–363 (2012)
40. Rahali, Y., Giorgio, I., Ganghoffer, J.F., dell'Isola, F.: Homogenization à la Piola produces second gradient continuum models for linear pantographic lattices. Int. J. Eng. Sci. **97**, 148–172 (2015)
41. Braides, A., Solci, M.: Interfacial energies on penrose lattices. Math. Models Methods Appl. Sci. **21**(5), 1193–1210 (2011)

42. Tomic, A., Grillo, A., Federico, S.: Poroelastic materials reinforced by statistically oriented fibres - numerical implementation and application to articular cartilage. IMA J. Appl. Math. **79**, 1027–1059 (2014)
43. Caggegi, C., Pensée, V., Fagone, M., Cuomo, M., Chevalier, L.: Experimental global analysis of the efficiency of carbon fiber anchors applied over cfrp strengthened bricks. Constr. Build. Mater. **53**, 203–212 (2014)
44. Tedesco, F., Bilotta, A., Turco, E.: Multiscale 3D mixed FEM analysis of historical masonry constructions. Eur. J. Environ. Civil Eng. (2016). doi:10.1080/19648189.2015.1134676
45. Turco, E., Rizzi, N.L.: Pantographic structures presenting statistically distributed defects: numerical investigations of the effects on deformation fields. Mech. Res. Commun. (submitted) (2016)
46. Turco, E.: Tools for the numerical solution of inverse problems in structural mechanics: review and research perspectives. Eur. J. Environ. Civil Eng. (2016). doi:10.1080/19648189.2015.1134673
47. Lekszycki, T., Olhoff, N., Pedersen, J.J.: Modelling and identification of viscoelastic properties of vibrating sandwich beams. Compos. Struct. **22**(1), 51–31 (1992)
48. Bilotta, A., Turco, E.: A numerical study on the solution of the Cauchy problem in elasticity. Int. J. Solids Struct. **46**, 4451–4477 (2009)
49. Bilotta, A., Morassi, A., Turco, E.: Reconstructing blockages in a symmetric duct via quasi-isospectral horn operators. J. Sound Vib. **366**, 149–172 (2016)
50. Bilotta, A., Turco, E.: Numerical sensitivity analysis of corrosion detection. Math. Mech. Solids (2014). doi:10.1177/1081286514560093
51. Alessandrini, G., Bilotta, A., Formica, G., Morassi, A., Rosset, E., Turco, E.: Evaluating the volume of a hidden inclusion in an elastic body. J. Comput. Appl. Math. **198**(2), 288–306 (2007)
52. Alessandrini, G., Bilotta, A., Morassi, A., Turco, E.: Computing volume bounds of inclusions by EIT measurements. J. Sci. Comput. **33**(3), 293–312 (2007)
53. Turco, E.: Identification of axial forces on statically indeterminate pin–jointed trusses by a nondestructive mechanical test. Open Civil Eng. J. **7**, 50–57 (2013)
54. Buffa, F., Cazzani, A., Causin, A., Poppi, S., Sanna, G.M., Solci, M., Stochino, F., Turco, E.: The Sardinia Radio Telescope: a comparison between close range photogrammetry and FE models. Math. Mech. Solids (2015) doi:10.1177/1081286515616227
55. Stochino, F., Cazzani, A., Poppi, S., Turco, E.: Sardinia Radio Telescope finite element model updating by means of photogrammetric measurements. Math. Mech. Solids (2015) doi:10.1177/1081286515616046
56. Del Vescovo, D., Giorgio, I.: Dynamic problems for metamaterials: review of existing models and ideas for further research. Int. J. Eng. Sci. **80**, 153–172 (2014)
57. Cazzani, A., Stochino, F., Turco, E.: On the whole spectrum of Timoshenko beams. Part I: a theoretical revisitation. Zeitschrift für Angewandte Math. Und Physik **67**(24), 1–30 (2016)
58. Cazzani, A., Stochino, F., Turco, E.: On the whole spectrum of Timoshenko beams. Part II: further applications. Zeitschrift für Angewandte Math. Und Physik **67**(25), 1–21 (2016)
59. Turco, E., dell'Isola, F., Rizzi, N.L., Grygoruk, R., Müller W., N., Liebold, C.: Fiber rupture in sheared planar pantographic sheets: numerical and experimental evidence. Mech. Res. Commun. **76**, 86–90 (2016)
60. D'Annibale, F., Rosi, G., Luongo, A.: Linear stability of piezoelectric-controlled discrete mechanical systems under nonconservative positional forces. Meccanica **50**(3), 825–839 (2015)
61. Gabriele, S., Rizzi, N.L., Varano, V.(2012) On the imperfection sensitivity of thin-walled frames. In: Topping, B.H.V. (ed.) Proceedings of the Eleventh International Conference on Computational Structures Technology, vol 99. doi:10.4203/ccp.99.15, Stirlingshire, UK, 2012. Civil-Comp Press.
62. Pignataro, M., Ruta, G., Rizzi, N.L., Varano, V.: Effects of warping constraints and lateral restraint on the buckling of thin-walled frames. ASME Int. Mech. Eng. Congr. Expo. **10**, 803–810 (2010)
63. Rizzi, N., Varano, V., Gabriele, S.: Initial postbuckling behavior of thin-walled frames under mode interaction. Thin-Walled Struct. **68**, 124–134 (2013)
64. Gabriele, S., Rizzi, N., Varano, V.: A 1D higher gradient model derived from Koiter's shell theory. Math. Mech. Solids **21**(6), 737–746 (2016)
65. AminPour, H., Rizzi, N.: A one-dimensional continuum with microstructure for single-wall carbon nanotubes bifurcation analysis. Math. Mech. Solids **21**(2), 168–181 (2016)
66. Gabriele, S., Rizzi, N.L., Varano, V.: A 1D nonlinear TWB model accounting for in plane cross-section deformation. Int. J. Solids Struct. **94–95**, 170–178 (2016)
67. AminPour, H., Rizzi, N.L.: On the continuum modelling of carbon nano tubes. In: Kruis, J., Tsompanakis, Y., Topping, B.H.V. (eds.) Proceedings of the 15th International Conference on Civil, Structural and Environmental Engineering Computing, vol. 108. Civil-Comp Press, Stirlingshire (2015)
68. Gabriele, S., Rizzi, N.L., Varano, V.: A one-dimensional nonlinear thin walled beam model derived from Koiter shell theory. In: Topping, B.H.V., Iványi, P. (eds.) Proceedings of the 12th International Conference on Computational Structures Technology. Civil-Comp Press, Stirlingshire (2014)

69. AminPour, H., Rizzi, N.L., Salerno, G.: A one-dimensional beam model for single-wall carbon nano tube column buckling. In: Topping, B.H.V., Iványi, P. (eds.) Proceedings of the 12th International Conference on Computational Structures Technology, vol. 106. Civil-Comp Press, Stirlingshire (2014)
70. Rizzi, N.L., Varano, V.: On the postbuckling analysis of thin-walled frames. In: Topping, B.H.V., Tsompanakis, Y. (eds.) Proceedings of the 13th International Conference on Civil, Structural and Environmental Engineering Computing. Civil-Comp Press, Stirlingshire (2011)

Emilio Turco
Department of Architecture
Design and Urban planning (DADU)
University of Sassari
Alghero, Sassari
Italy
e-mail: emilio.turco@uniss.it

Katarzyna Barcz and Marek Pawlikowski
Institute of Mechanics and Printing
Warsaw University of Technology
Warsaw
Poland
e-mail: k_barcz@o2.pl;
m.pawlikowski@wip.pw.edu.pl

Nicola Luigi Rizzi
Department of Architecture
Roma Tre University
Rome
Italy
e-mail: nicolaluigi.rizzi@uniroma3.it

(Received: August 14, 2016)